Figures and figure supplements

Selection and the direction of phenotypic evolution

François Mallard *et al.*

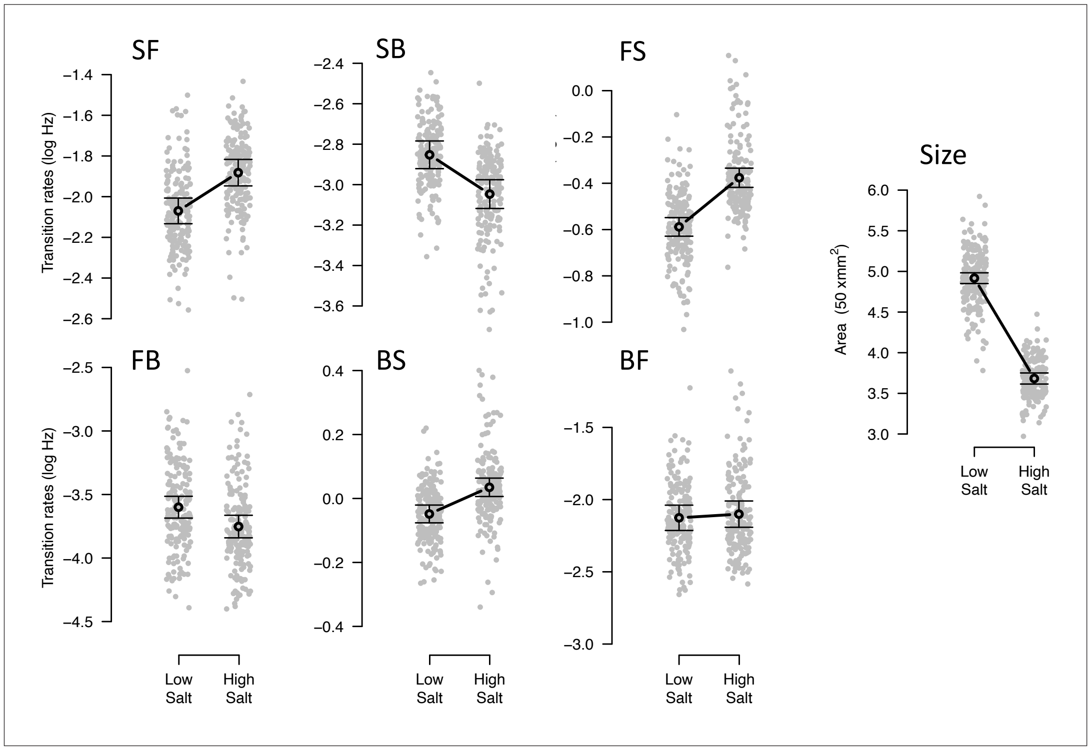

Figure 1. Phenotypic plasticity of the ancestral population. Gray dots indicate the trait values (BLUPs) estimated for each inbred line in the low and high salt environments: F for 'forward,' B for 'backward', and S for 'still,' left to right order indicating movement direction. Gray circles and bars indicate the mean 95% confidence intervals least-square estimates using the univariate approach (see Methods). Significant differences between environments are indicated with a line, when using the multivariate approach (***Table 2***). Figure source code is linked here - Multivariate analysis of variance (MANOVA) and figures/tables export scripts.

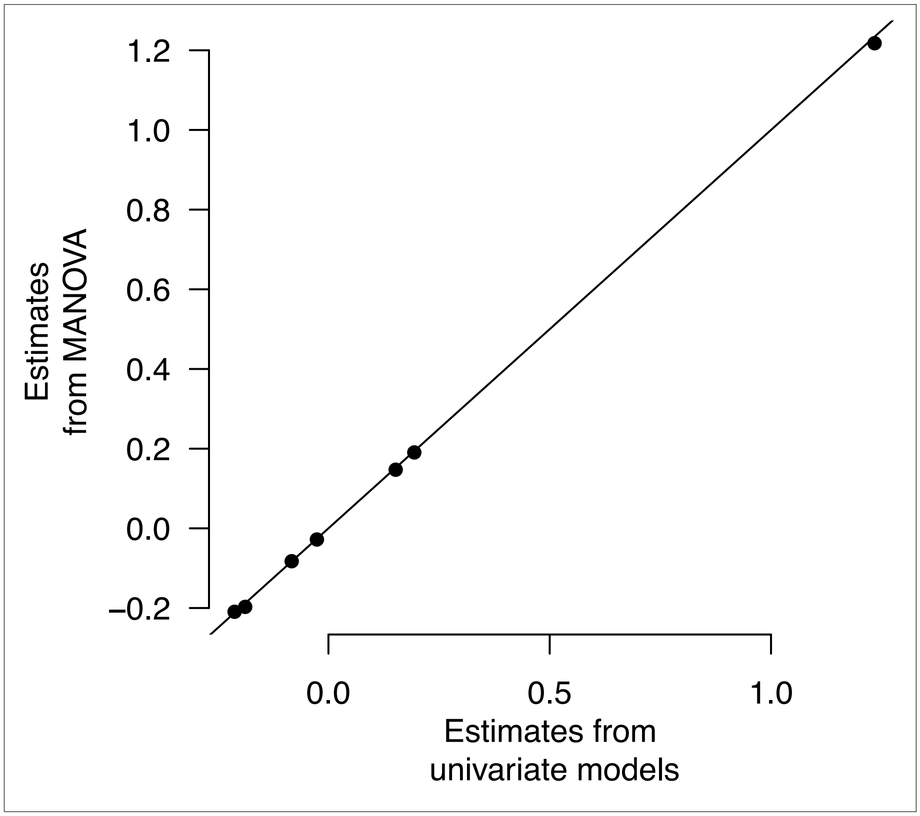

Figure 1—figure supplement 1. Multivariate and univariate models' environmental effects. The least-square mean estimates of high salt environmental effects for each of the seven traits in the ancestral population are shown.

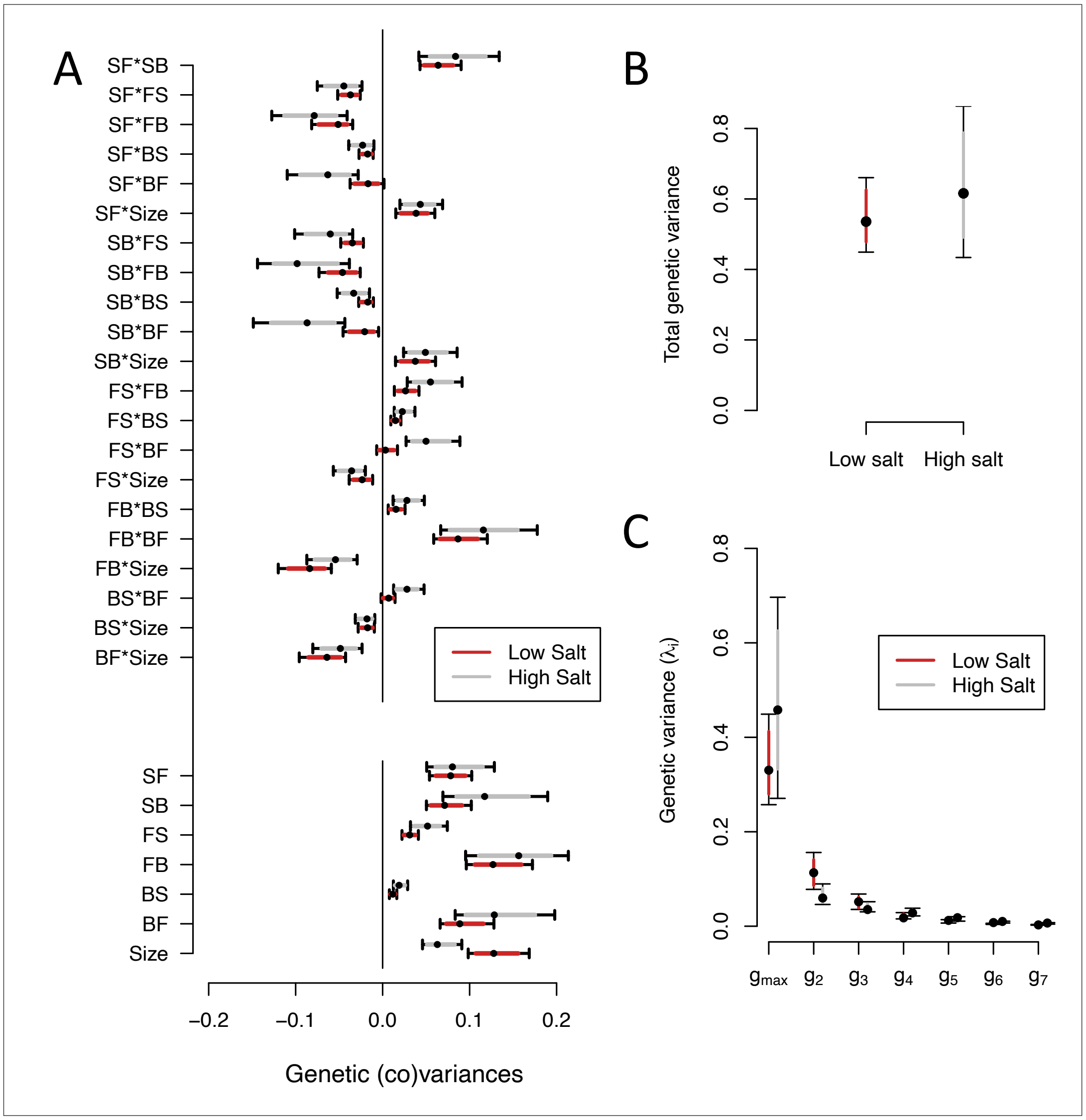

Figure 2. G-matrix of the ancestral population in low salt and high salt environments. (**A**). The bottom seven estimates indicate the genetic variances in transition rates and body size, top 15 estimates are the genetic covariances between the seven traits. (**B**). Total genetic variance in each environment is the trace of the G-matrices (**C**). Eigenvalues of the six eigenvectors for each G-matrix. For all panels, red (gray) indicates estimates in low (high) salt, with dots, and colored intervals the mode and the 83% or 95% credible intervals of the posterior distribution.

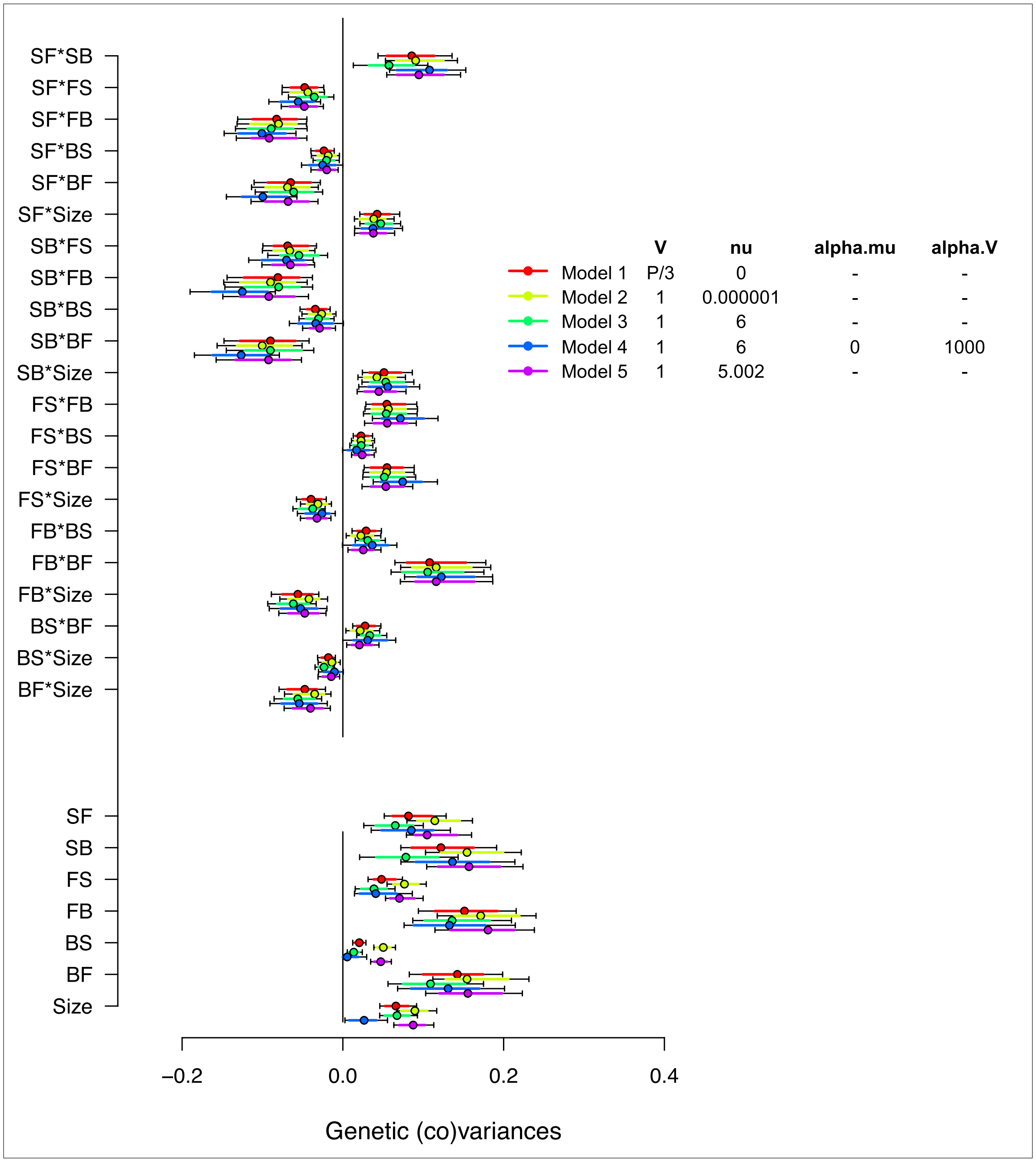

Figure 2—figure supplement 1. Varying priors for G-matrix estimation in the ancestral population. Varying prior distributions for G-matrix estimation. Inset shows the parameters used to specify the priors for all matrices estimated with the *MCMCglmm* model (i.e. both random effect matrices and the residual). V is the expected value and nu the 'degree of belief' for the Inverse-Wishart distribution. Model 1 uses a flat improper prior, retained for all analysis. Models 2, 3, and 5 use inverse-Wishart distributions as priors with different degrees of belief. Model 4 uses parameter-expanded algorithms with $alpha.mu$ and $alpha.V$ being the prior means and covariances, respectively. Dots show the modes with 83% and 95% of the posterior high salt G-matrix distribution.

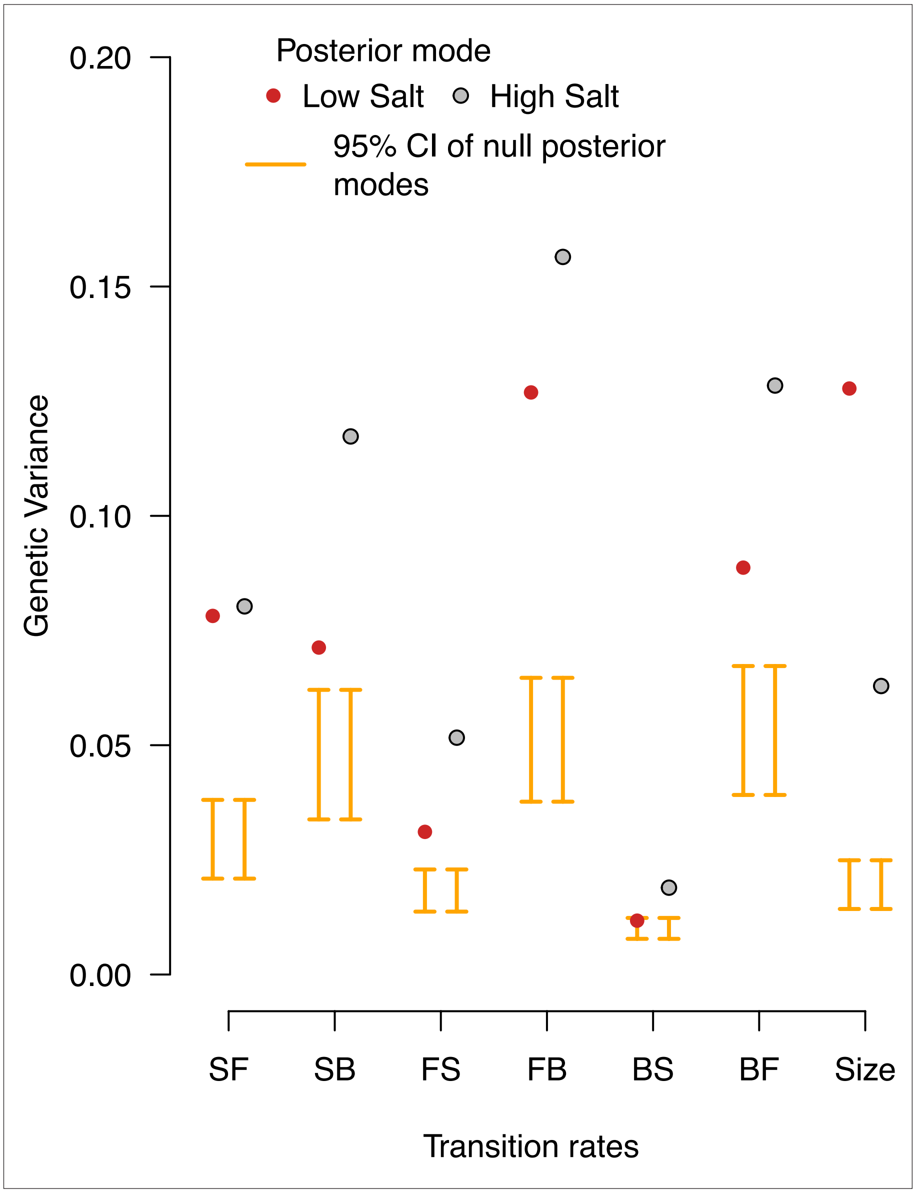

Figure 2—figure supplement 2. Null distributions of genetic variances in the ancestral population. Genetic variance estimates in the ancestral population's low salt and high salt environments. The posterior modes are compared with 95% CI of the posterior modes distribution of 1,000 randomized G-matrices by inbred line and block identities (orange bars). Red (gray) indicates the posterior mode estimates in low (high) salt from ***Figure 2***.

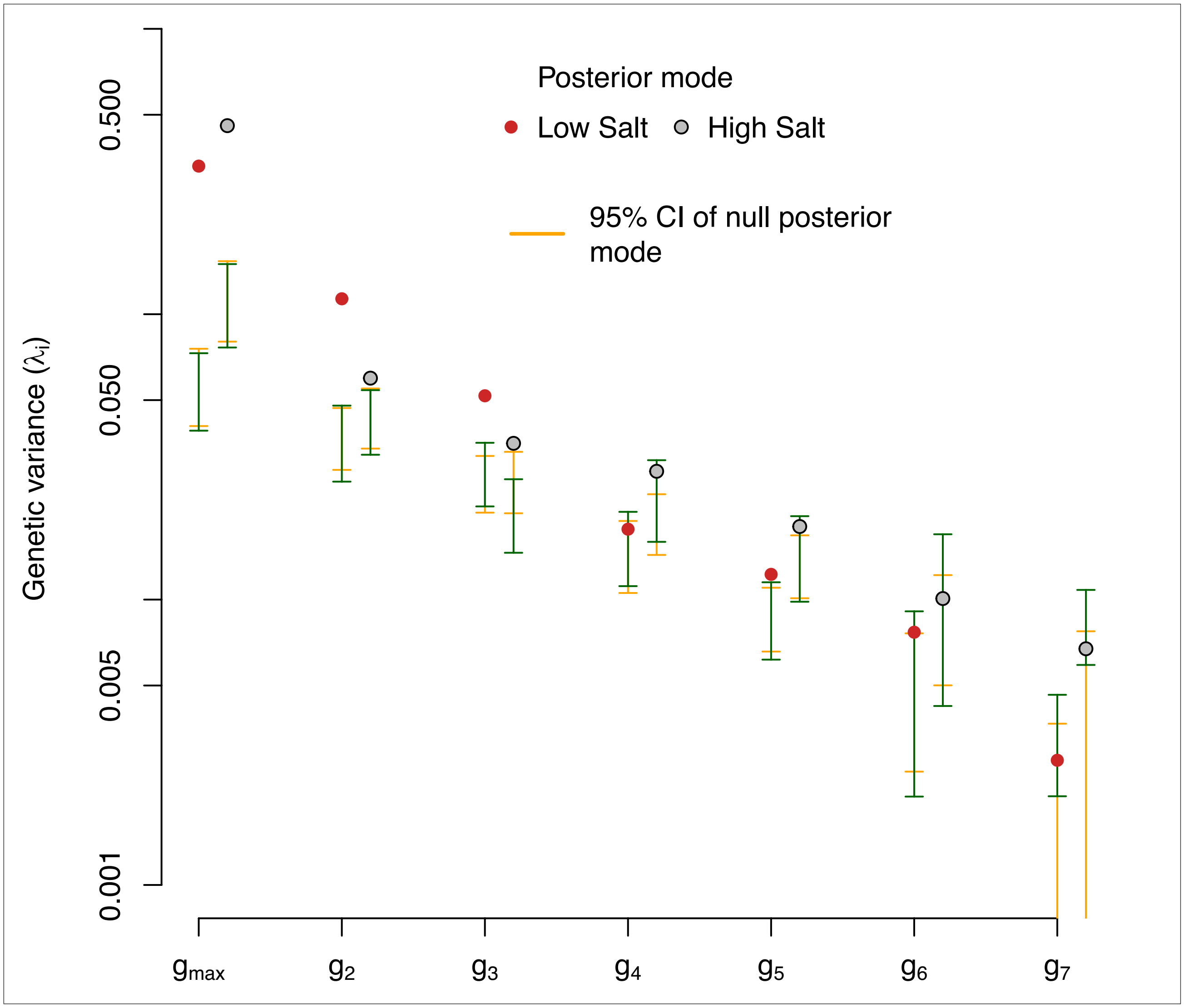

Figure 2—figure supplement 3. Eigendecomposition of null distributions of the ancestral G-matrix. G-matrix eigenvalues in low salt (red) and high salt (gray) environments for the ancestral population. The posterior modes are compared with the 95% CI of randomized G-matrices using two methods. Orange bars show the 95% CI of the distribution of posterior modes of 1000 randomized G-matrices. Green bars show the 95% CI posterior distribution of the genetic variance in the observed eigenvectors (***Figure 2A***).

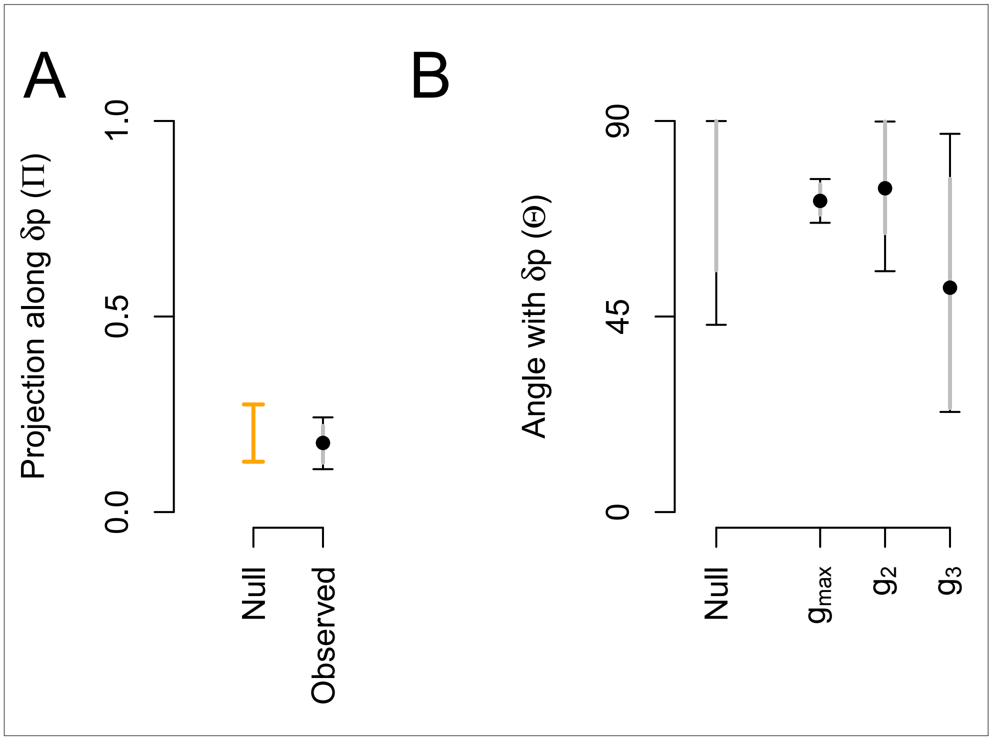

Figure 3. Aligment between phenotypic plasticity and standing genetic variation in high salt for the ancestral population. (**A**) Projection of the high salt G-matrix along the phenotypic plasticity canonical trait δp. Dots show the mean estimate with bars the 83% and 95% credible interval of the posterior G-matrix distribution. Orange bar shows the null 95% CI of the posterior distribution of modes of 1000 G-matrix randomized by inbred line and block identities (see Methods). (**B**). The angle (Θ, ***Equation 3***) between δp and the first three eigenvectors of the ancestral G-matrix (g_{max}, g_2, and g_3). Θ does not differ from the random expectations. Dots show the mean estimate with bars the 83% and 95% credible interval of the posterior G-matrix distribution. The null expectation was obtained by computing the angle between pairs of random vectors sampled from a uniform distribution (see Methods).

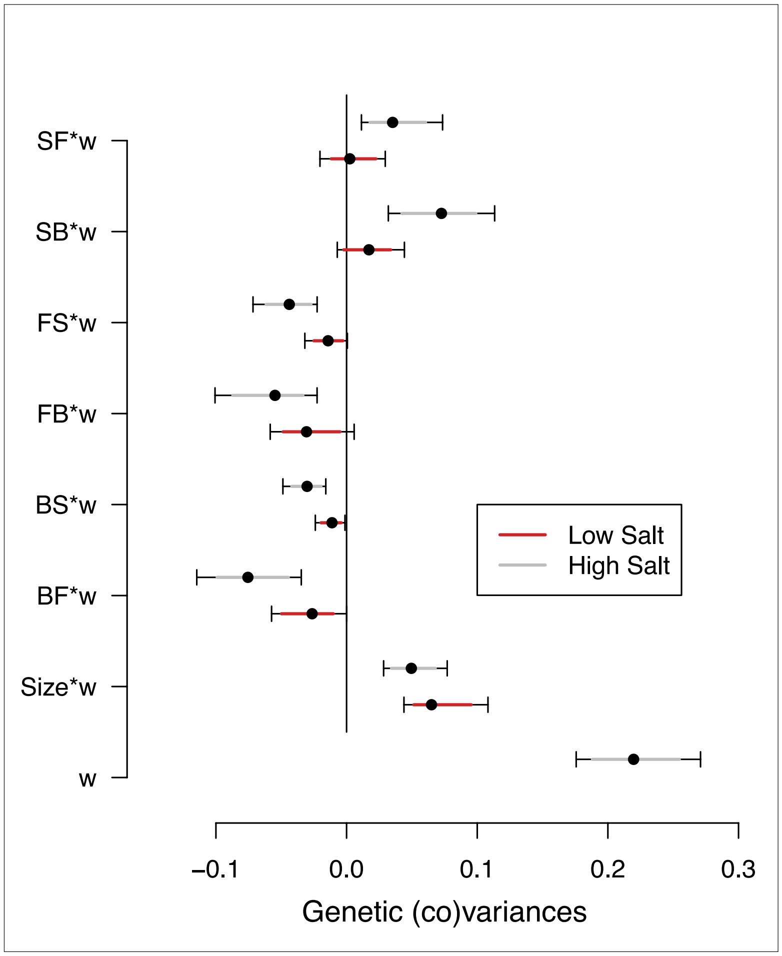

Figure 4. Selection differentials in the ancestral population. Ancestral genetic covariances between transition rates and body size measured in high salt (gray) or low salt (red) with high salt self-fertility. Dots and colored intervals show the mode and the 83% or 95% credible intervals of the posterior G_{qw} distribution.

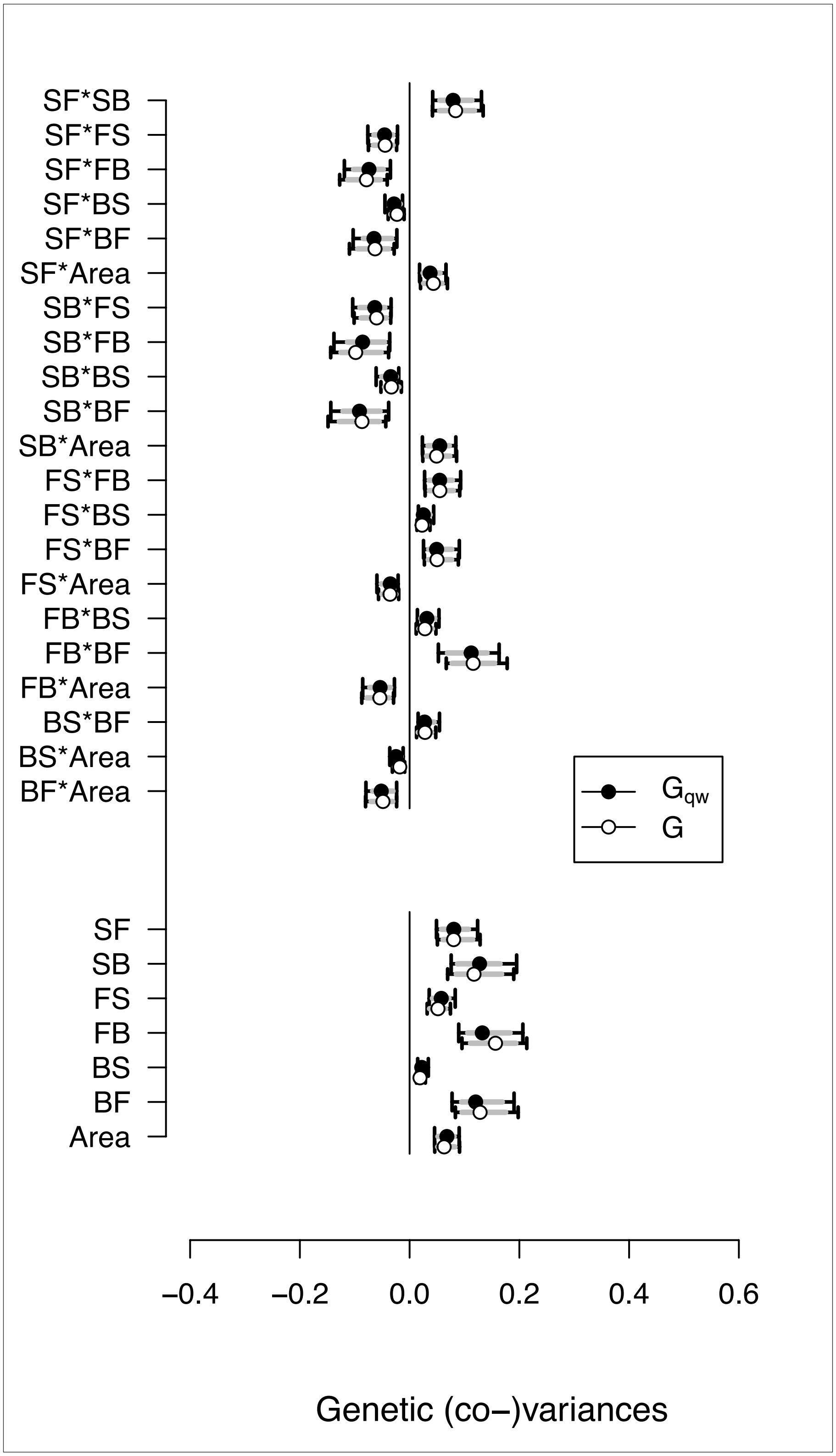

Figure 4—figure supplement 1. Genetic (co)variances estimate from the G- and G_{qw}-matrices. Selection differentials were estimated as the last column of the G_{qw}-matrix. This plot shows that the genetic (co)variance estimates of locomotion traits and body size are robust to adding an 8th trait (self-fertility) to the G-matrix. Circles show the mode and 83% and 95% CI of the posterior distributions.

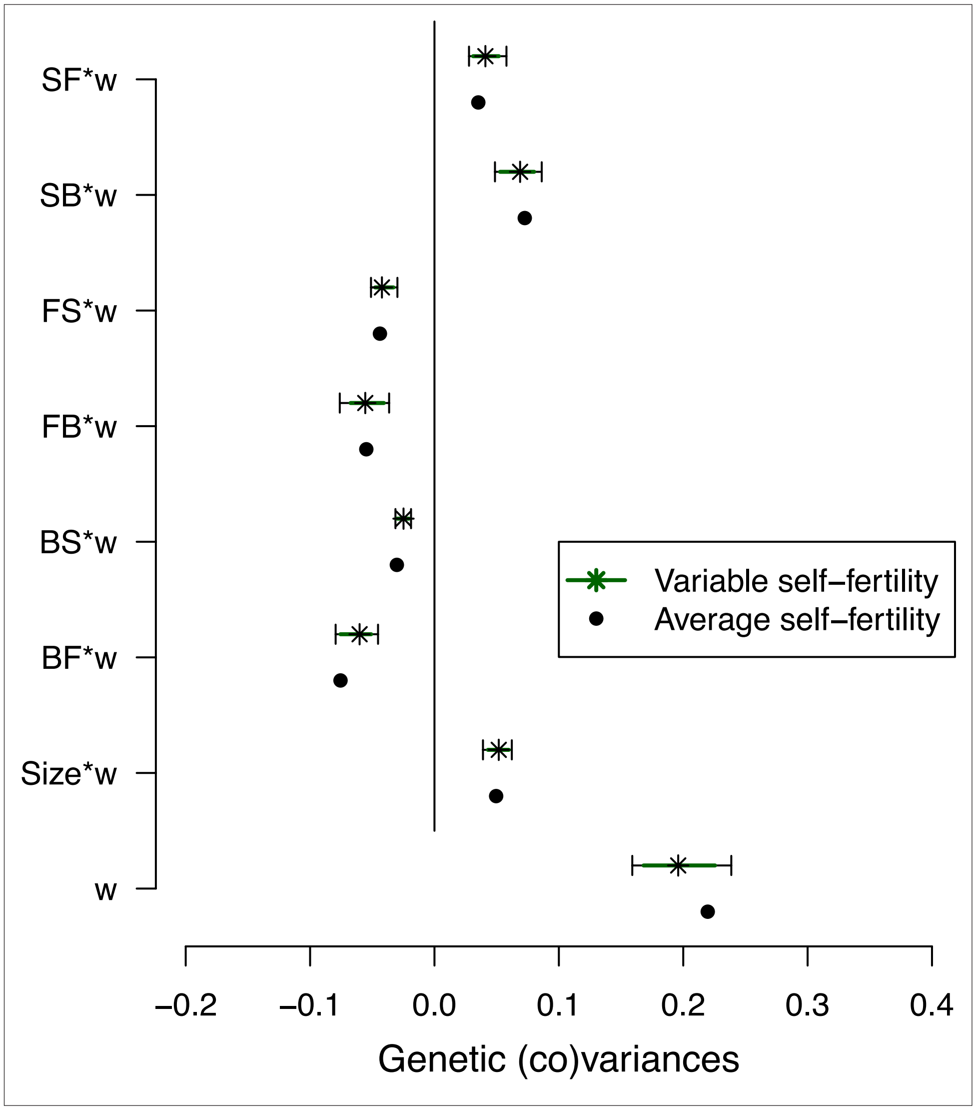

Figure 4—figure supplement 2. Self-fertility variation effects on selection differentials' estimates. Effect of self-fertility variation in selection differentials estimates for the ancestral population (high salt environment only). We generated 500 G_{qw} matrices while generating variable self-fertility measurements for each set of measured transition rates based on the standard deviation of the means estimates for each line fecundity (stars; see Methods). Dots show the mean posterior estimates (***Figure 4***).

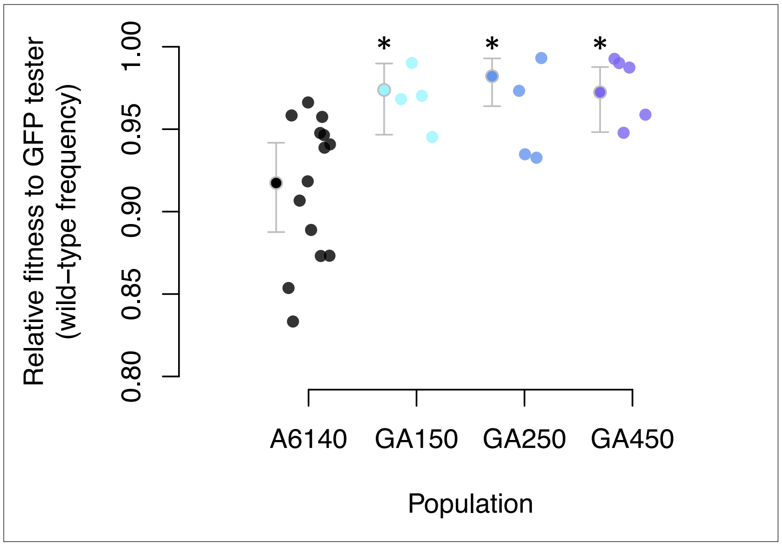

Figure 5. Adaptation to the high salt environment. Colored dots show the ratio of wild-type to green-fluorescent protein (GFP) alleles after one generation of pairwise competitions between the outbred experimental populations with a GFP-tester strain. Filled circles indicate the least-square mean estimates with 95% confidence intervals; asterisks indicate significant differences between each replicate population relative to the ancestral population.

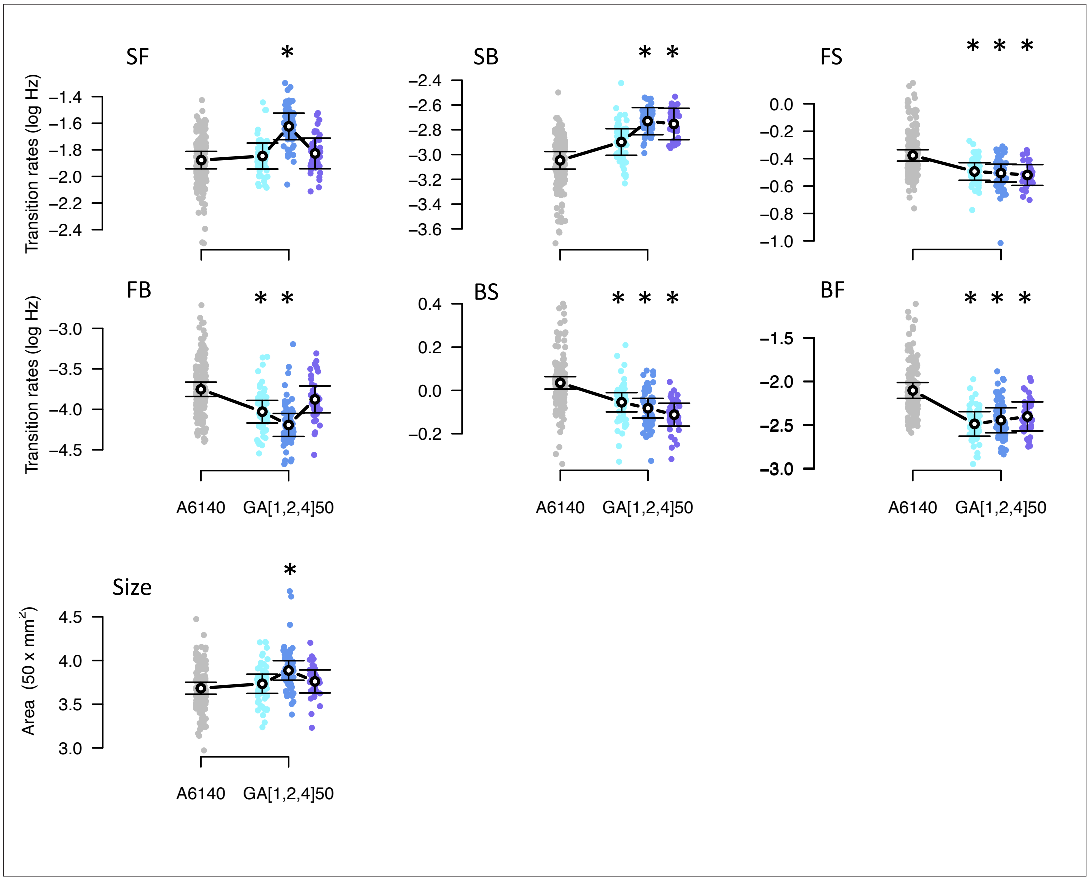

Figure 6. Phenotypic divergence in the high salt environment. Each panel shows the transition rates and body size as in ***Figure 1***. Dots indicate the values estimated for each inbred line in a high salt environment, gray for the ancestral population, blues for the evolved replicate populations. Circles and bars indicate the mean and the 95% confidence intervals least-square estimates. Line shows significant differentiation between all four populations using the multivariate MANOVA approach (***Table 2***). Significant differences between each of the evolved populations and the ancestral population using the univariate approach are shown with asterisks (***Figure 6—source data 2***).

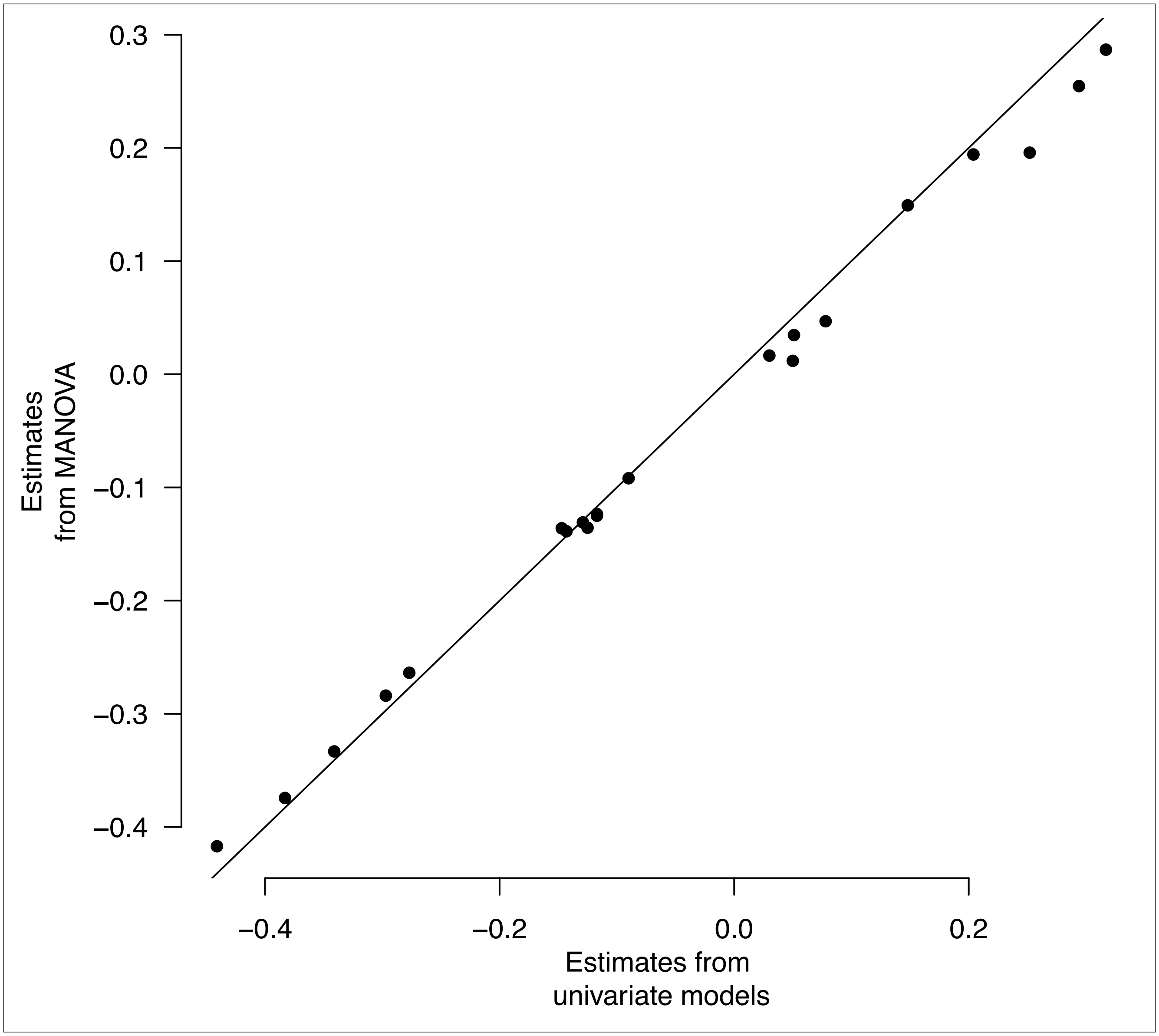

Figure 6—figure supplement 1. Multivariate and univariate models' population estimates. Multivariate and univariate models' population effects. Least-square mean estimates for each of the seven traits are plotted.

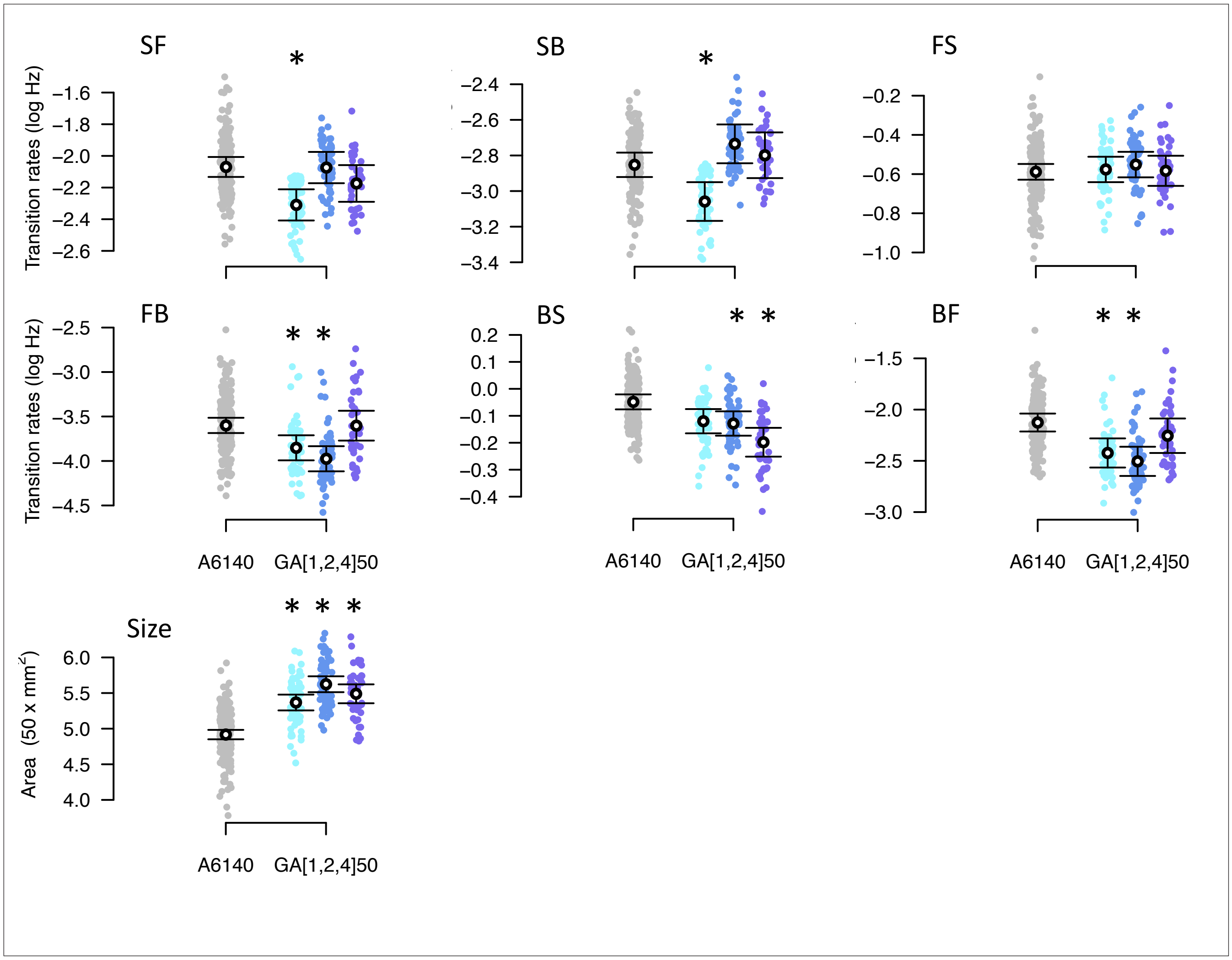

Figure 6—figure supplement 2. Phenotypic divergence in the low salt environment. Each panel shows the transition rates and body size. Dots indicate the values estimated for each inbred line, gray for the ancestral population, blues for the evolved GA populations. Circles and bars indicate the mean and the 95% confidence intervals least-square estimates. Significant differences between each evolved population relative to the ancestral population are shown with an asterisk, using the univariate modeling approach.

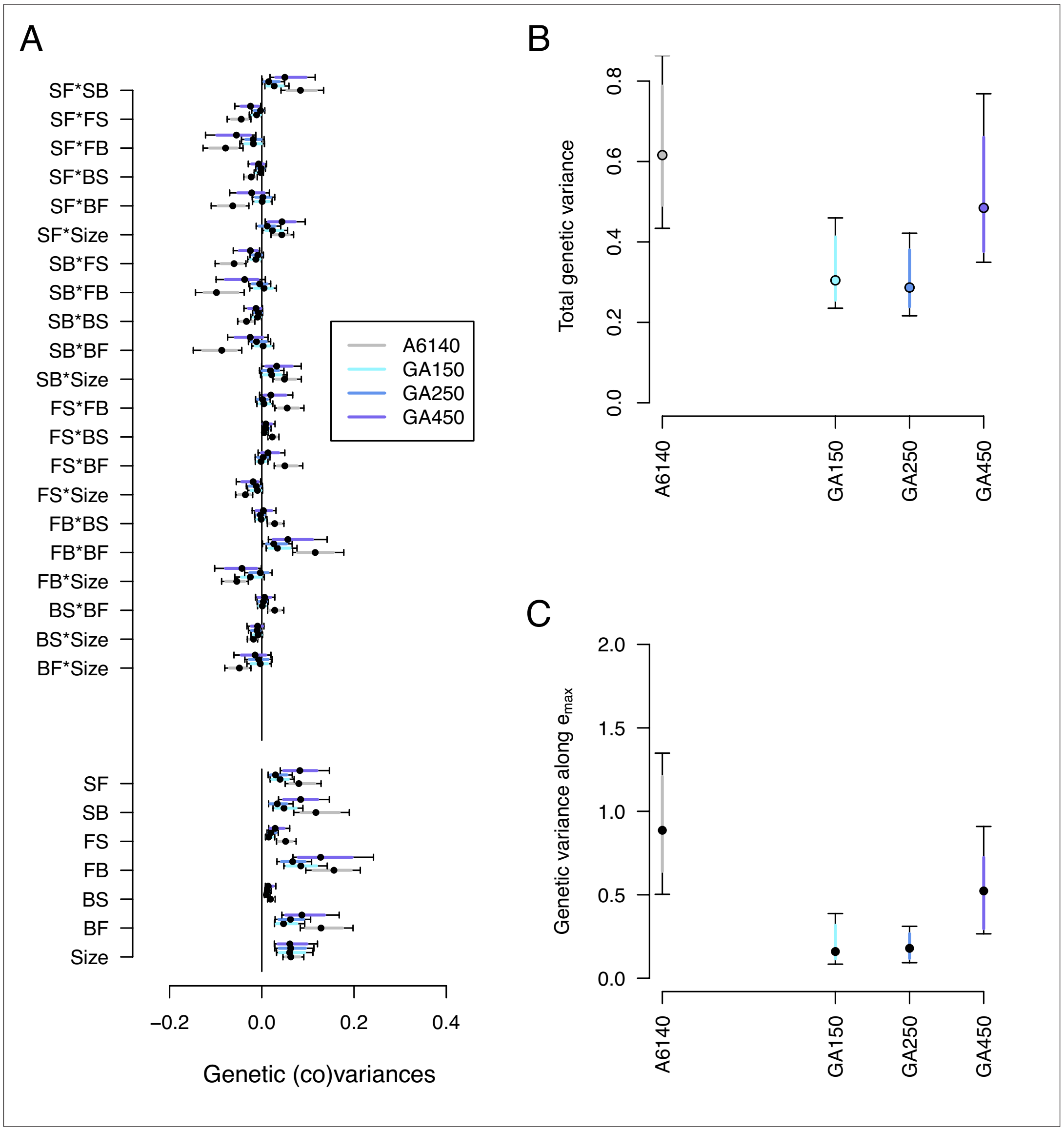

Figure 7. Genetic divergence in the high salt environment. (**A**) High salt G-matrix evolution of ancestral (gray) and evolved GA populations (blues). Eigendecomposition of the ancestral G-matrix (gray) can be found in ***Figure 2***, those of the evolved GA populations in ***Figure 7—figure supplement 2***. (**B**) Total G-matrix variance for each experimental population. (**C**) Genetic variance along e_{max}, the main canonical trait of genetic differentiation obtained after the random skewers analysis (see Methods, ***Table 1***). Dots and colored bars show the mode and the 83% or 95% credible intervals of the posterior distribution. Figure 7 sources linked here - matrix computation, random skewers analysis, and Figure 7 scripts. The Figure 7 scripts also produces all three figure supplements.

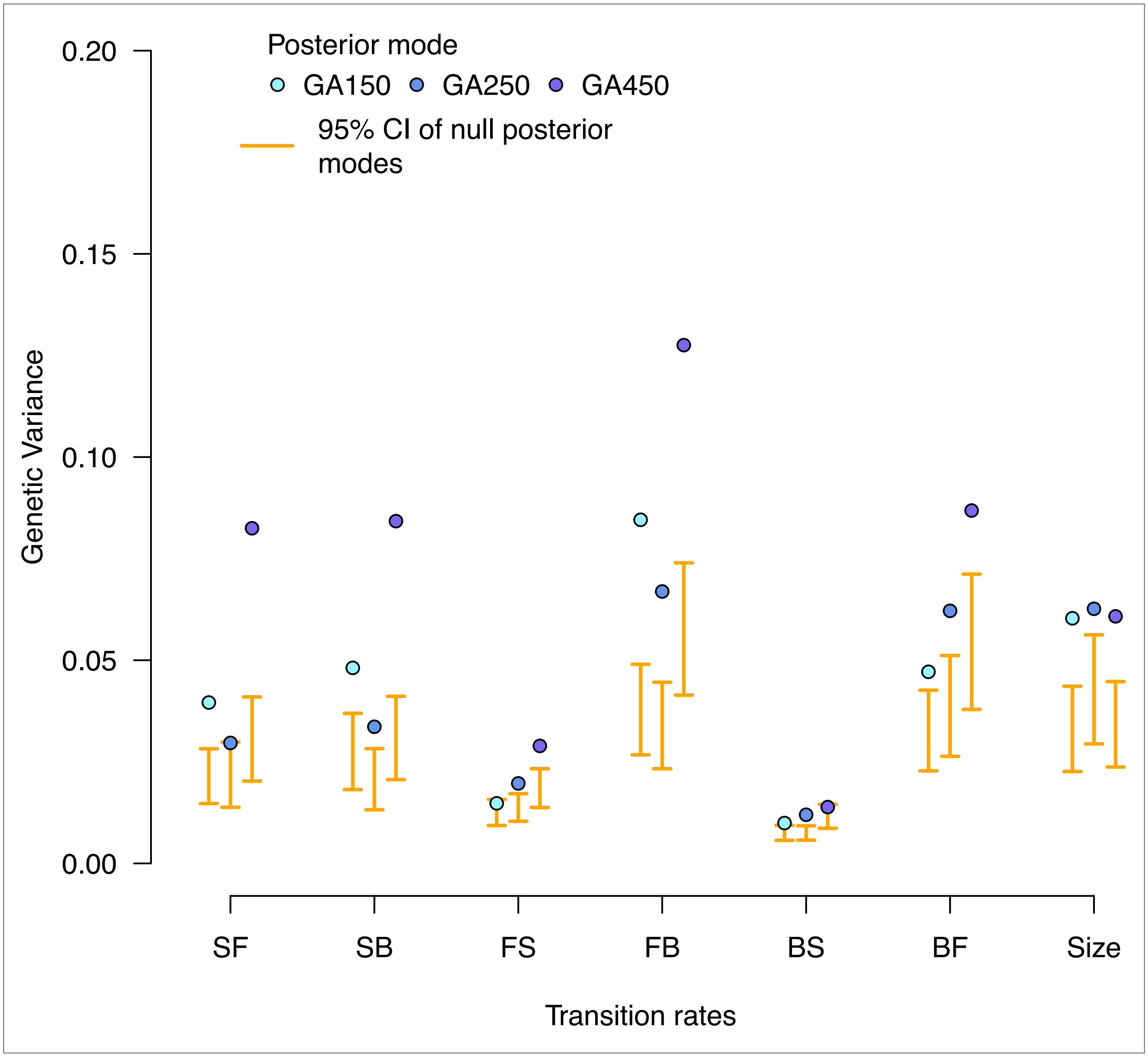

Figure 7—figure supplement 1. Null distributions of high salt genetic variances in the evolved populations. Genetic variance estimates for each experimentally evolved population in the high salt environment. Blue dots indicate the posterior mode for each replicate. These values are compared with the posterior mode distribution obtained from randomizing the G-matrices by inbred line and assay block identities (orange).

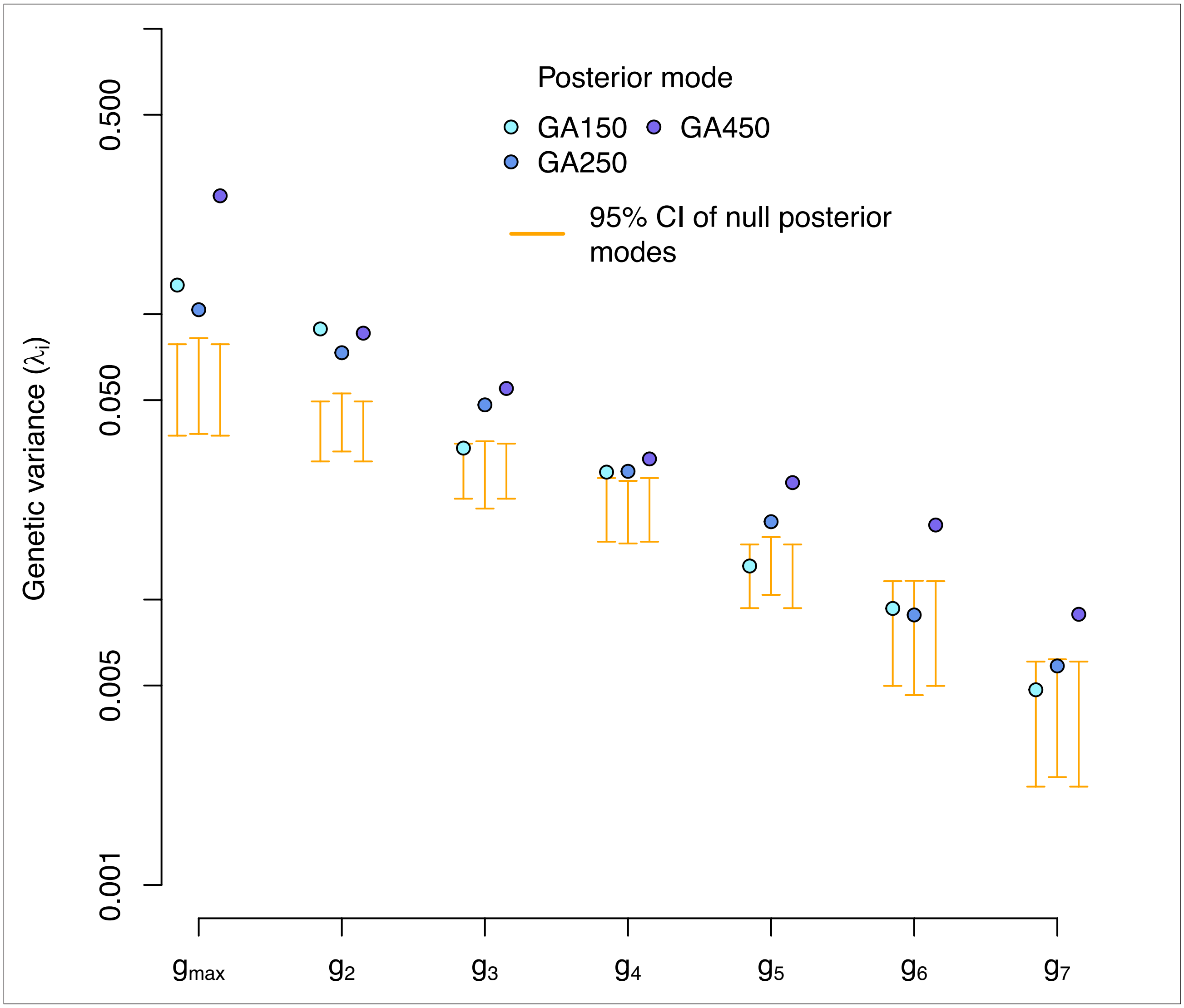

Figure 7—figure supplement 2. Eigendecomposition of the high salt G-matrix of the evolved populations. G-matrix eigenvalues for each experimentally evolved population in the high salt environment. Blue dots indicate the posterior mode for each replicate. These values are compared with the posterior mode distribution obtained from randomizing the G-matrices by inbred line and assay block identities (orange).

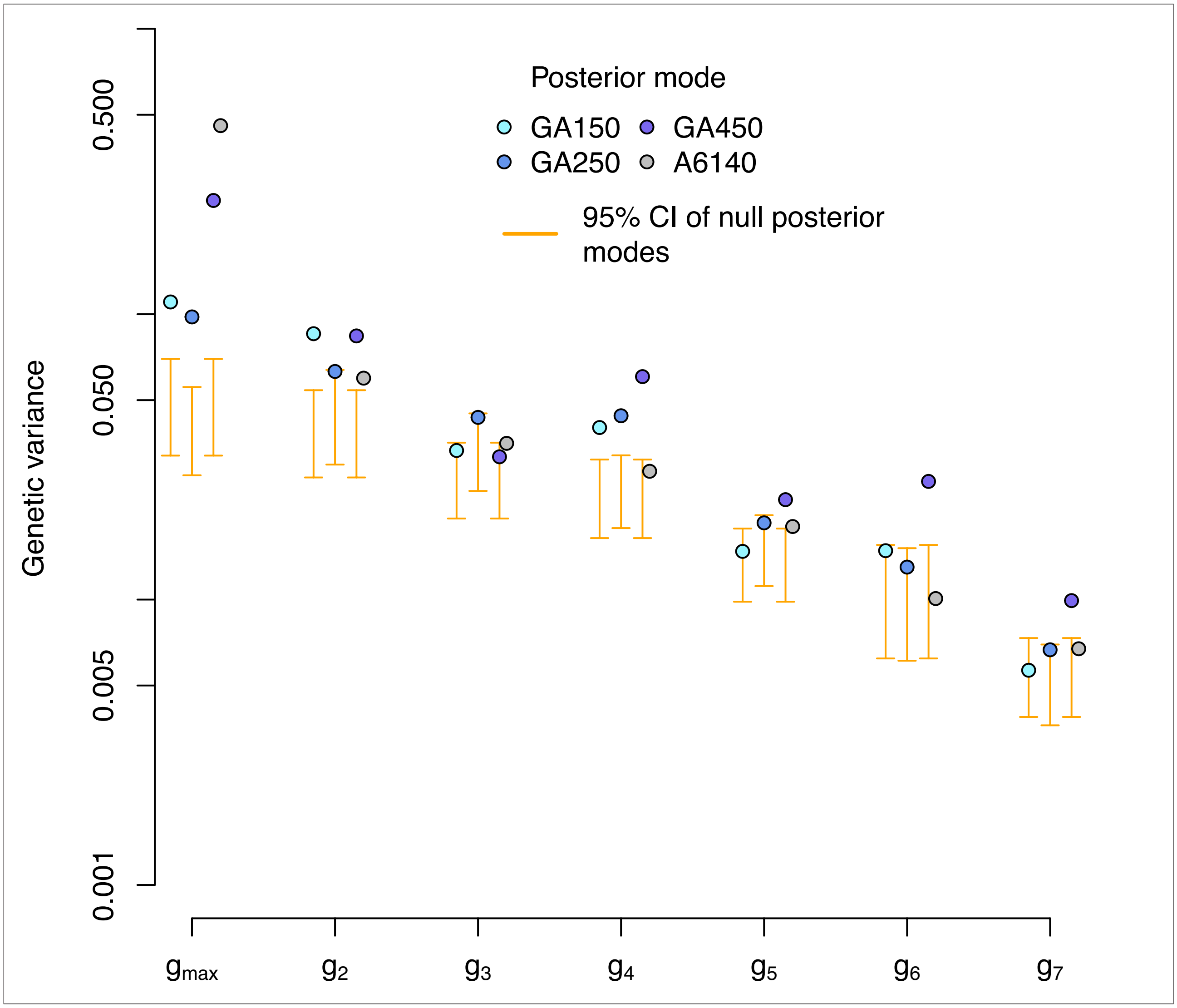

Figure 7—figure supplement 3. Genetic variance of the high salt G-matrix in the evolved populations along the eigentraits of the ancestral population. Genetic variance in the high salt environment for each experimentally evolved population and their ancestral population in the eigentraits of the ancestral populations. Blue and gray dots indicate the posterior mode for each replicate. These values are compared with the posterior mode distribution obtained from randomizing the G-matrices by inbred line and assay block identities (orange, for the evolved populations only).

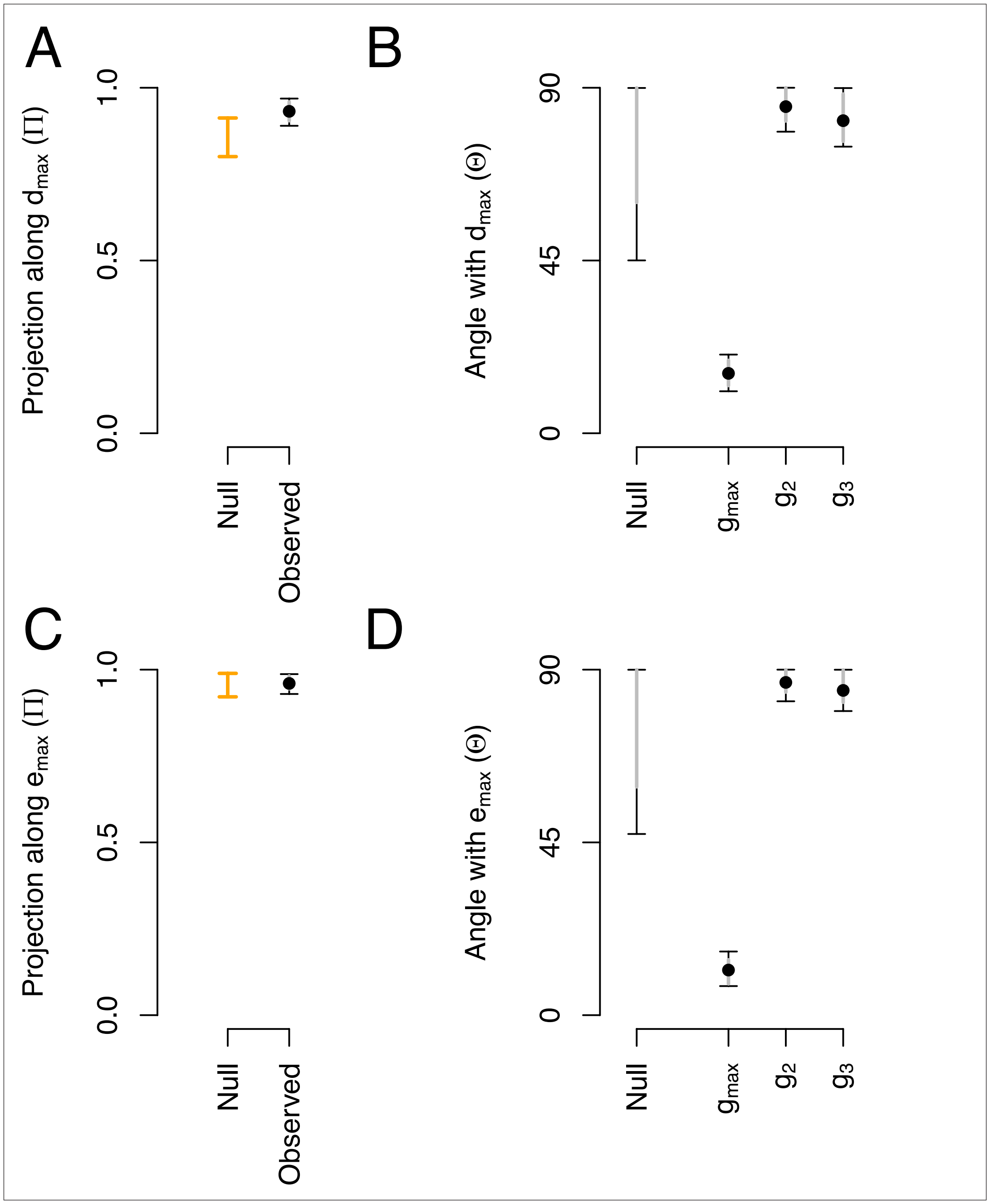

Figure 8. Phenotypic and genetic divergence alignments with ancestral standing variation. (**A**) Projection of the total ancestral genetic variance along the phenotypic divergence canonical trait d_{max}. Dots show the mean estimate with bars the 95% CI. Orange bar shows the null 95% CI after randomizing the G-matrix (see Methods). Mean of the observed posterior distribution (0.93) is outside the 95% CI of the randomized posterior modes (0.80–0.91). (**B**). The angle (Θ) between d_{max} and the first three eigenvectors of the ancestral G-matrix ($g_{max,2,3}$). The null expectation was obtained by computing the angle between 1000 pairs of random vectors. (**C and D**) Similar projection and angles as shown in (**A**) and (**B**) but with e_{max} - the vector of the main genetic divergence - instead of d_{max}. In (**C**), the null and observed projections do not differ. Because e_{max} and g_{max} are almost aligned, both the observed and the null are very close to one (as Π is estimated relatively to λ_{max}, see ***Equation 5***) and the relative phenotypic variance between traits is conserved in the randomized G-matrices.

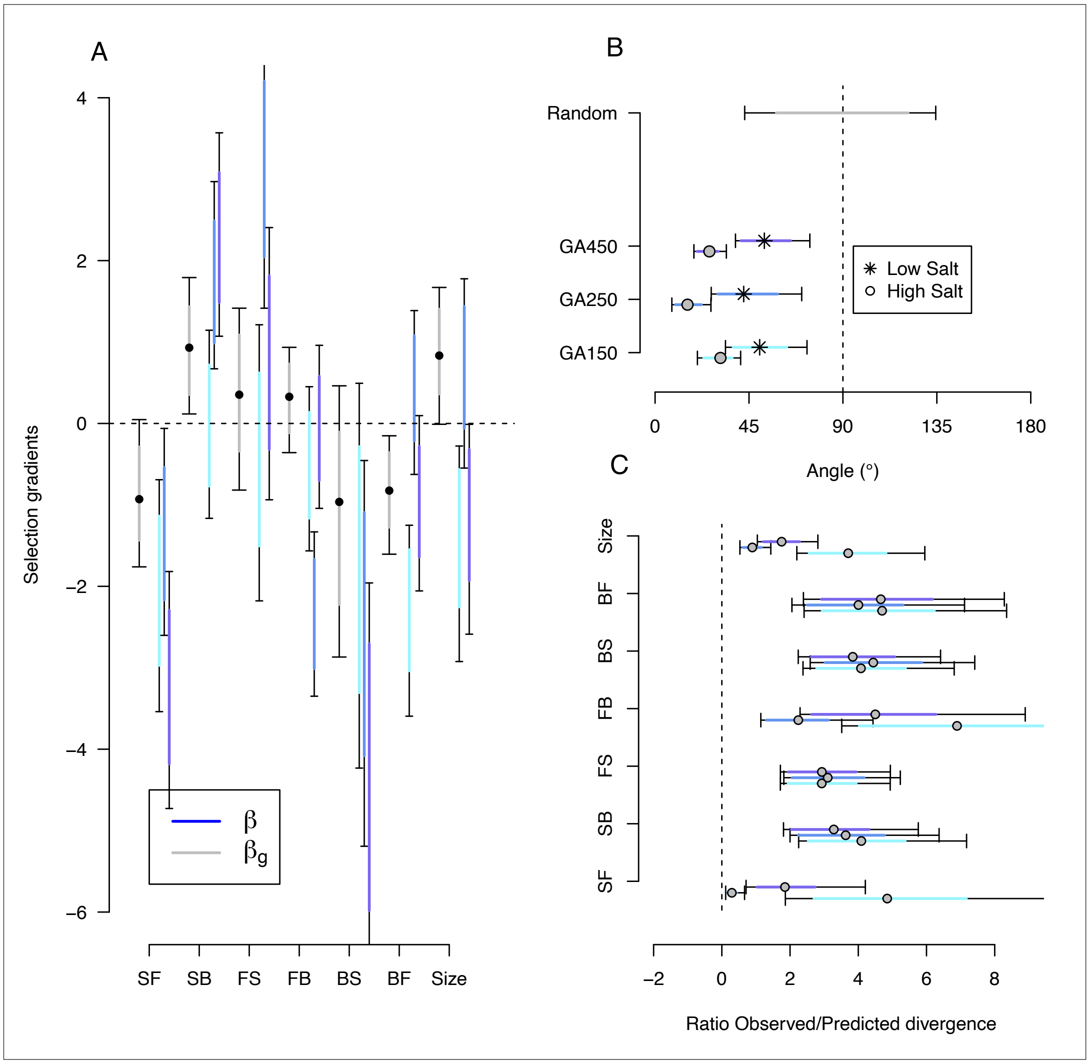

Figure 9. Predicting phenotypic evolution with Lande's equation. (**A**) Indirect and direct selection. Genetic selection gradients β_g (gray) and phenotypic selection gradients β (blues) for each replicate population, see ***Equation 6*** and ***Equation 7***, respectively. β were divided by 3.5 for scaling (the average ratio observed/predicted divergence, panel C) rather than by 140 (the total number of generations in the experiment) for visual convenience. (**B**) The direction of phenotypic evolution. Angle between the expected phenotypic divergence (selection differentials, s_k; ***Figure 4***) and the observed phenotypic divergence at each replicate ($\Delta\bar{q}_k$; ***Figure 6***). Circles show the results in the high salt environment and stars in the low salt environment. The expected angle by chance is in gray and was generated by computing 1000 angles between pairs of randomly generated vectors from a uniform distribution $\mathcal{U}^7(-1,1)$. (**C**) The magnitude of phenotypic evolution. The ratio phenotypic divergence at each replicate ($\Delta\bar{q}_k$) with expected divergence (s_k). For all panels, dots/circles/stars and colored bars show the mode and the 83% or 95% credible intervals of the posterior distributions obtained by sampling in posterior distribution of the ancestral high salt G-matrix (***Figure 2***).

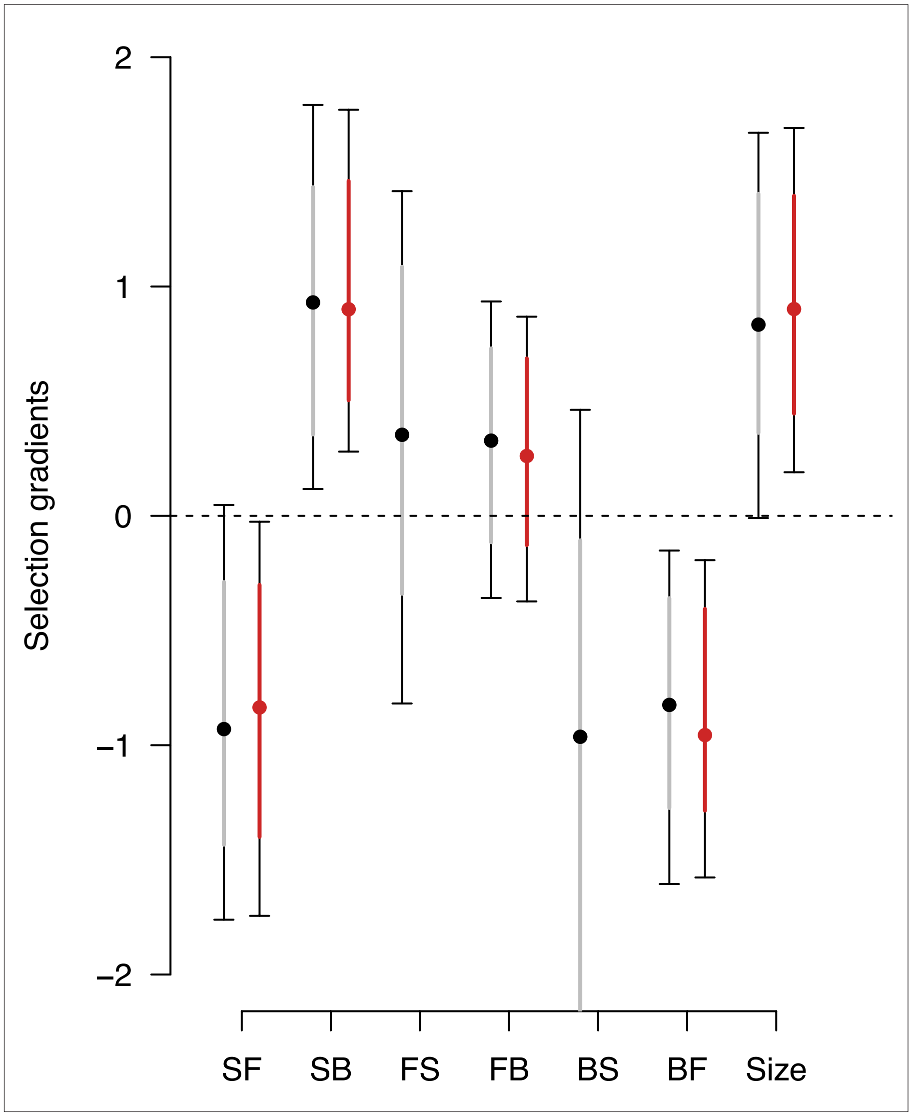

Figure 9—figure supplement 1. Genetic selection gradients bias due to low variance traits. Estimates of genetic selection gradients β_g, as in ***Figure 9***, obtained by sampling the posterior distribution of the ancestral high salt G-matrix with (gray) or without (red) traits with low genetic variance (from ***Figure 2—figure supplement 2***, the forward-to-still (FS) and back-to-still (BS) traits).

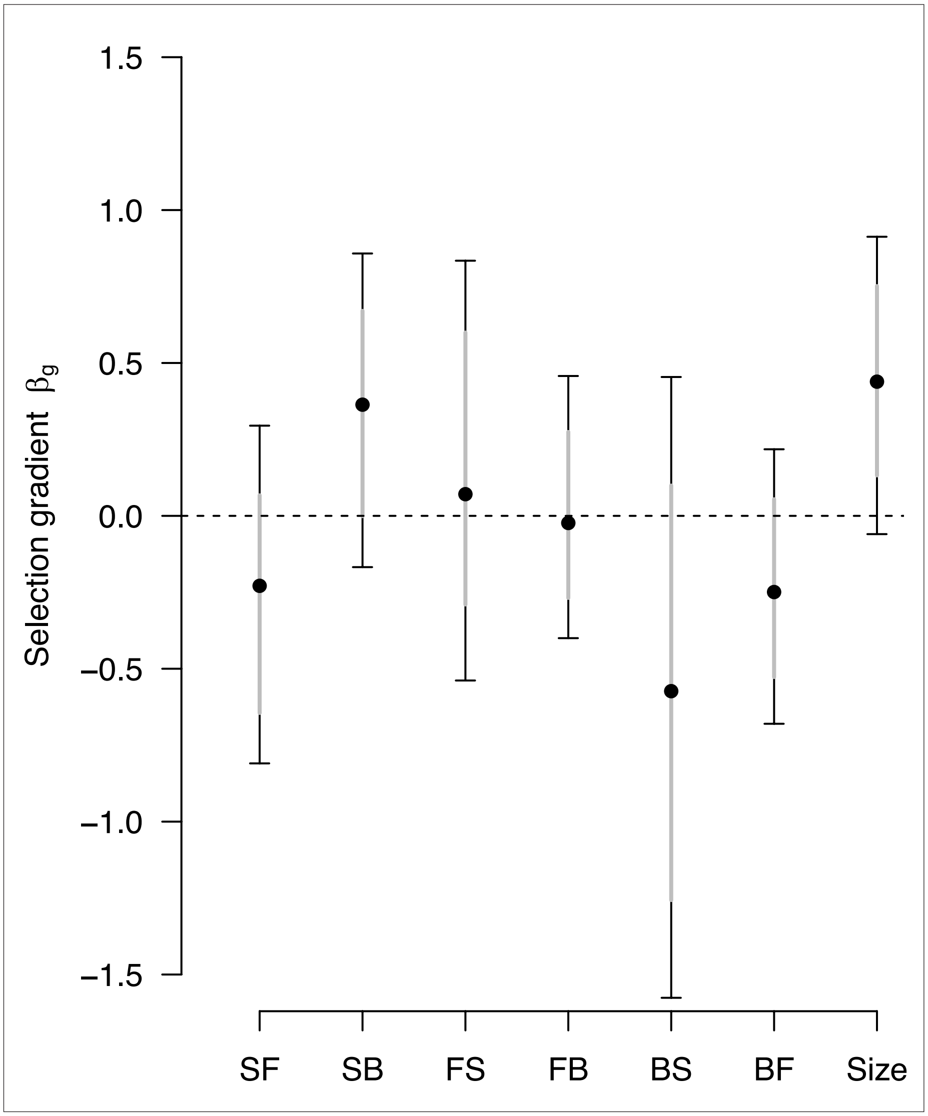

Figure 9—figure supplement 2. Genetic selection gradients with a sampling of G-matrix and differentials. Estimates of genetic selection gradients β_g, as in ***Figure 9***, obtained by sampling the posterior distribution of the ancestral high salt G-matrix and the posterior distribution of s_k.